GEOPHYSICS. VOL. 76, NO. 6 (NOVEMBER-DECEMBER 2011); P. H1–H18, 19 FIGS., 1 TABLE.
10.1190/GEO2010-0039.1

Finite-difference modeling experiments for seismic interferometry

Jan W. Thorbecke[1] and Deyan Draganov[1]

ABSTRACT

In passive seismic interferometry, new reflection data can be retrieved by crosscorrelating recorded noise data. The quality of the retrieved reflection data is, among others, dependent on the duration and number of passive sources present during the recording time, the source distribution, and the source strength. To investigate these relations we set up several numerical modeling studies. To carry out the modeling in a feasible time, we design a finite-difference algorithm for the simulation of long-duration passive seismic measurements of band-limited noise signatures in the subsurface. Novel features of the algorithm include the modeling of thousands of randomly placed sources during one modeling run. The modeling experiments explore the dependency relation between the retrieved reflections and source-signature length, source positions, number of sources, and source amplitude variations. From these experiments we observed that the positions of the passive sources and the length of the source signals are of direct influence on the quality of the retrieved reflections. Random amplitude variations among source signals do not seem to have a big impact on the retrieved reflections.

INTRODUCTION

Seismic interferometry (SI) is a relatively new branch of geophysics and deals with the retrieval of new seismic responses between receivers by crosscorrelating responses recorded at these receiver locations. Applications of SI exist for exploration data with controlled sources (Schuster et al., 2004; Bakulin et al., 2004, 2006; Wapenaar, 2006), as well as for passive data due to natural sources (Rickett and Claerbout, 1999; Wapenaar et al., 2002; Draganov et al., 2007). For a cross-discipline overview, we refer the readers to the Geophysics Reprint Series about SI (Wapenaar et al. (editors), 2008), which also contains contributions from authors from other disciplines. The retrieval of surface waves using natural sources has already led to numerous successful studies (e.g. Campillo and Paul [2003]; Shapiro and Campillo [2004]). SI for the retrieval of reflected body waves from passive measurements has been successfully applied only recently (Draganov et al., 2007, 2009). However, in many cases it remains difficult to interpret the retrieved wavefields and verification with modeled or measured results remains useful.

To test ideas and new concepts for SI, aiming at the retrieval of reflected body waves, passive measurements are needed. Despite the many advantages that SI could offer, passive measurements are still rare and for the moment, we have to rely on numerical forward-modeling studies to gain experience in the practical use of passive SI. The goal of the modeling studies discussed in this paper, and carried out by the specially designed algorithm, is to get a better understanding of what influences the quality of the retrieved reflections. In the following sections we give insights to the relation between the quality of the retrieved reflections and:

- the average duration of the passive sources;
- the number of the passive sources captured during the recording time;
- the source distribution;
- the presence of intrinsic attenuation in the medium;
- variations in the passive-source amplitudes;
- the effect of receiver topography.

This list is by no means complete and represents first steps in studying and quantifying the quality of retrieved reflections. For the simulation of passive measurements, very long recording times are needed (from minutes to hours), many (thousands) of random source positions, random source signatures, and random excitation times have to be included in the modeling algorithm. Without the software, presented as a part of this paper, we would not have been able to perform all the experiments discussed in the following sections. Along with the discussion about the experiments, implementation aspects of the algorithm are explained as well. To guide the

Peer-reviewed code related to this article can be found at http://software.seg.org/2011/0001.
Manuscript received by the Editor 28 January 2010; revised manuscript received 10 June 2011; published online 28 December 2011.
[1]Delft University of Technology, Department of Geotechnology, Delft, Netherlands. E-mail: J.W.Thorbecke@tudelft.nl; d.s.draganov@tudelft.nl.

reader, Table 1 lists the kind of experiment carried out and the figure number showing the results of the experiment.

We start this paper by briefly reviewing the Green's function representation for SI with two-way wavefields. The first example in the "Modeling Experiments" section illustrates the basic concepts of SI. We use the result in that example as a reference for comparison with subsequent retrieved SI results. We then continue by presenting the results for different variations of random source positions and source signatures and investigate their connection to the quality of the retrieved reflection data. We will also explain how these experiments can be carried out using the accompanying software. The manual, bundled with the software, should be consulted for more detailed explanations about the parameter settings to use. The last section shows SI results for a more complicated model and includes topography. In the Appendix, the finite-difference algorithm and the generation and implementation of band-limited random-noise signals is explained.

SI WITH TWO-WAY WAVEFIELDS

In the brief theoretical background given in this section, we show the main relations for SI as derived by Wapenaar and Fokkema (2006) from reciprocity theory. Consider a Green's function $G(\mathbf{x}, \mathbf{x}_A, t)$ for an inhomogeneous lossless acoustic medium, where $\mathbf{x}$ and $\mathbf{x}_A$ are the Cartesian coordinate vectors for the observation and source points, respectively, and where t denotes time. We define the temporal Fourier transform as $\hat{G}(\mathbf{x}, \mathbf{x}_A, \omega) = \int_{-\infty}^{\infty} \exp(-j\omega t)\, G(\mathbf{x}, \mathbf{x}_A, t)\mathrm{d}t$, where j is the imaginary unit and ω the angular frequency. Assuming the unit point source at $\mathbf{x}_A$ is of the volume-injection-rate type, the wave equation for acoustic pressure $\hat{G}(\mathbf{x}, \mathbf{x}_A, \omega)$ reads

$$\rho\partial_i((1/\rho(\mathbf{x}))\partial_i\hat{G}(\mathbf{x}, \mathbf{x}_A, \omega)) + (\omega^2/c^2(\mathbf{x}))\hat{G}(\mathbf{x}, \mathbf{x}_A, \omega) = -j\omega\rho\delta(\mathbf{x} - \mathbf{x}_A). \tag{1}$$

Here $c(\mathbf{x})$ and $\rho(\mathbf{x})$ are the propagation wavespeed and the mass density of the inhomogeneous medium and ∂_i denotes the partial derivative in the x_i-direction (Einstein's summation convention applies to repeated subscripts). In the remainder of this section we will leave out the dependency on frequency in the notation of the Green's functions $\hat{G}$. The representation of $\hat{G}$, as derived for SI from Rayleigh's reciprocity theorem (Rayleigh, 1878; Bojarski, 1983; Wapenaar et al., 2004, 2005), reads

Table 1. The different experiments carried out and the figure number showing the results.

Experiment	Figure number
source duration	Figure 4
number of sources	Figure 5 and 6
source distribution	Figure 7, 8, and 9
attenuation	Figure 10
source amplitude	Figure 12 and 13
receiver topography	Figure 15

$$\hat{G}_h(\mathbf{x}_A, \mathbf{x}_B) = \oint_{\partial\mathbb{D}} \frac{-1}{j\omega\rho(\mathbf{x})}(\hat{G}^*(\mathbf{x}_A, \mathbf{x})\partial_i\hat{G}(\mathbf{x}_B, \mathbf{x}) - (\partial_i\hat{G}^*(\mathbf{x}_A, \mathbf{x}))\hat{G}(\mathbf{x}_B, \mathbf{x}))n_i\mathrm{d}^2\mathbf{x}, \tag{2}$$

with

$$\hat{G}_h(\mathbf{x}_A, \mathbf{x}_B) = \hat{G}(\mathbf{x}_A, \mathbf{x}_B) + \hat{G}^*(\mathbf{x}_A, \mathbf{x}_B) = 2\Re\{\hat{G}(\mathbf{x}_A, \mathbf{x}_B)\}, \tag{3}$$

where $\partial\mathbb{D}$ is an arbitrary closed surface with an outward pointing normal vector $\mathbf{n} = (n_1, n_2, n_3)$ and the asterisk denotes complex conjugation. The points $\mathbf{x}_A$ and $\mathbf{x}_B$ are both situated inside $\partial\mathbb{D}$; the medium may be inhomogeneous inside as well as outside $\partial\mathbb{D}$. Note that equation 2 is exact and applies to any lossless arbitrary inhomogeneous acoustic medium. The retrieved Green's function $\hat{G}(\mathbf{x}_A, \mathbf{x}_B)$ contains, apart from the direct wave between $\mathbf{x}_A$ and $\mathbf{x}_B$, all scattering contributions including primary and multiple reflections from inhomogeneities inside as well as outside $\partial\mathbb{D}$.

To make equation 2 more suited for practical applications, several approximations are made: The medium at and outside $\partial\mathbb{D}$ is assumed to be homogeneous, with propagation velocity c and mass density ρ; a far-field approximation expresses the dipole sources in terms of scaled monopoles; the medium parameters around $\partial\mathbb{D}$ are assumed to be smoothly varying (Wapenaar and Fokkema, 2006). These approximations lead to the following equation

$$2\Re\{\hat{G}(\mathbf{x}_A, \mathbf{x}_B)\} \approx \frac{2}{c\rho}\oint_{\partial\mathbb{D}} \hat{G}^*(\mathbf{x}_A, \mathbf{x})\hat{G}(\mathbf{x}_B, \mathbf{x})\mathrm{d}^2\mathbf{x}. \tag{4}$$

In general, these approximations involve amplitude errors that can be significant (Ramirez and Weglein, 2009). Furthermore, spurious events may occur due to incomplete cancellation of contributions from different stationary points when the medium outside $\partial\mathbb{D}$ is inhomogeneous (Draganov et al., 2004). However, since the approximations do not affect the phase of equation 4, it is considered acceptable for SI.

When we assume that the sources are uncorrelated (both in space and in time) we can write the observed wavefields as

$$\hat{u}^{\mathrm{obs}}(\mathbf{x}_A) = \oint_{\partial\mathbb{D}} \hat{G}(\mathbf{x}_A, \mathbf{x})\hat{N}(\mathbf{x})\mathrm{d}^2\mathbf{x} \quad \text{and}$$
$$\hat{u}^{\mathrm{obs}}(\mathbf{x}_B) = \oint_{\partial\mathbb{D}} \hat{G}(\mathbf{x}_B, \mathbf{x})\hat{N}(\mathbf{x})\mathrm{d}^2\mathbf{x}, \tag{5}$$

where the noise spectrum $\hat{N}(\mathbf{x}, \omega)$ has to fulfill

$$\langle\hat{N}(\mathbf{x})\hat{N}^*(\mathbf{x}')\rangle = \delta(\mathbf{x} - \mathbf{x}')\hat{S}(\omega), \tag{6}$$

where $\langle . \rangle$ denotes a spatial ensemble average and $\hat{S}(\omega)$ the power spectrum of the noise sources. Equation 6 states that $\hat{N}(\mathbf{x})$ and $\hat{N}(\mathbf{x}')$ are mutually uncorrelated for any $\mathbf{x} \neq \mathbf{x}'$ at $\partial\mathbb{D}$, and that their power spectrum $\hat{S}(\omega)$ is the same for all x. Using equations 5 and 6 in equation 4 results in

$$2\Re\{\hat{G}(\mathbf{x}_A, \mathbf{x}_B)\}\hat{S}(\omega) \approx \frac{2}{c\rho}\langle\hat{u}^{\mathrm{obs}*}(\mathbf{x}_A)\hat{u}^{\mathrm{obs}}(\mathbf{x}_B)\rangle. \tag{7}$$

If part of $\partial\mathbb{D}$ is formed by a free surface ($\partial\mathbb{D}_0$), then in equation 4 and 5 we will need sources only of the part $\partial\mathbb{D}_1 = \partial\mathbb{D} - \partial\mathbb{D}_0$ that

does not include the free surface (see Figure 1). When the receivers $\mathbf{x}_A$ and $\mathbf{x}_B$ are placed on the free surface, equation 7 remains valid and the observed quantities u^{obs} are then particle velocities (Wapenaar and Fokkema, 2006). We use equations 7 and 5 in the remainder of this paper to retrieve reflection data from passive measurements.

MODELING EXPERIMENTS

The modeling experiments in this section investigate how retrieved reflections depend on different passive-source configurations. At the same time, it illustrates the capabilities of the finite-difference algorithm bundled with the paper. To get an idea of how well the reflections could be retrieved with passive SI, we would like to compare the results that we obtain with an active SI reference result obtained using a regular distribution of transient sources along a closed contour (shown as a dashed line in Figure 2) around particle-velocity receivers placed at the free surface. A source is placed at every grid point on this dashed line, with a grid spacing of 10 m. The sources are modeled sequentially using a loop to start a new FD modeling for each source position. The source signal is a first derivative of a Gaussian wavelet with a frequency peak at 13 Hz. The receivers are placed on the free surface at $z = 0$ on a 50 m grid covering the whole surface. This experiment follows the theory as close as possible according to interferometry equation 4.

Figure 3 shows the contribution of the different parts of the closed contour to the retrieved reflections. Figure 3a shows the contribution of sources placed on the lower horizontal part ($z = 3600$ m) of the contour. This result shows that the higher angles in the reflection response are missing, but all reflections and multiples are already present. The contribution of the two vertical parts of the closed contour in Figure 3b mainly retrieves the higher angles of the reflections. Outside and close to the upper part of the vertical edges of the chosen contour the assumptions in equation 4 are violated, and spurious events can be observed. In Figure 3b these spurious events are clearly visible outside the integration contour, between $-5000 : -4000$ and $4000 : 5000$ m and exhibit a reverse curvature of the reflection arrivals. The contribution of the complete closed contour is shown in Figure 3c and we can see, as expected, a successful retrieval of all reflection events. For comparison, in Figure 3d a directly forward-modeled result is shown.

Influence of the number of sources and source-signature length

As a first SI experiment with passive sources, we use again the model shown in Figure 2 but with random source positions below level $z = 500$ m. In Figure 2 the source positions, in total 1000, are shown as black dots. In the algorithm a square region, where the sources can be placed, is defined by the four corners using the parameters `xscr1`, `xsrc2`, `zsrc1`, `zsrc2`. For the investigation of the sources' influence on the retrieved result, the source signal duration and start time is varied, while the source strength is the same for all sources. The source signature is a random sequence with a maximum frequency of 30 Hz and constructed according to the procedure explained in the Appendix. The FD program

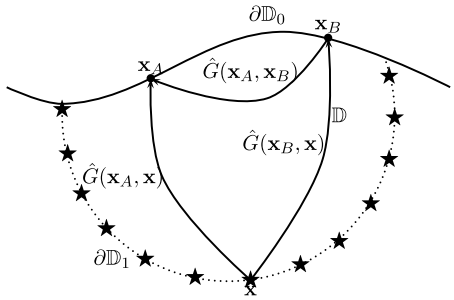

Figure 1. Green's function ($\hat{G}$) retrieval by crosscorrelation requires sources (★) on a closed surface. When part of the closed surface is a free surface ($\partial\mathbb{D}_0$), it suffices to have sources on the remaining part ($\partial\mathbb{D}_1$). The rays represent the full responses, including primary and multiple scattering due to inhomogeneities and reflections from the free surface $\partial\mathbb{D}_0$.

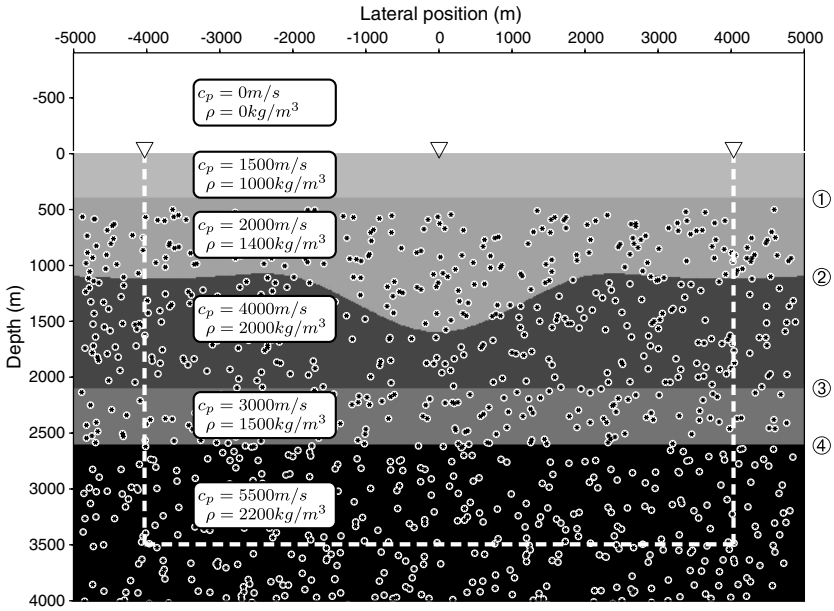

Figure 2. Sources with a noise signature are positioned at random locations, visible as black dots, within the model. At $z = 0$ a free surface is implemented and the receivers are placed on the free surface. The dashed line indicates source positions on a closed integral with regularly distributed transient sources. The ▽ represent the receiver positions placed at every 50 m.

simulates all 1000 sources in one run of the program (see section one of the code manual for more details). In FD modeling, a wavefield at all gridded x, z positions is modeled for a next time step given the wavefield at the current time step. If an active time window of a source is encountered during the time stepping of the algorithm, the source amplitude of that time step is added to the wavefield at the grid position of the source. This multisource implementation allows to model many different experiments within a reasonable computational time. The duration and noise signature of the sources in the presented experiments are not based on actual measurements and observations. The chosen maximum frequency is based on actual measurements, however (Draganov et al., 2007, 2009).

Figure 4a shows again the reference retrieved result of Figure 3d: a shot record for a source position in the middle of the model. Figure 4b–4f show retrieved results using a total recording time of 120 seconds. The noise-source signature duration varies between zero and 120 s, 60 s, 30 s, 10 s, and 5 s in Figure 4b–4f, respectively. The sources are activated at a random moment in the time interval 0–120 s. Starting at $t = 0$ no sources will be active, but during the modeling many sources will become active and sources will also be active simultaneously.

At the end of the FD modeling, the middle trace is correlated with all the output traces to compute the SI result. From Figure 4 it is clear that longer source signatures give a more complete retrieval of the reflections. Note also that only the strongest reflectors in the model are visible through the uncorrelated events. Free-surface and internal multiples occur after 2.0 s and can be observed in the reference result, but in the retrieved results they are not readily visible because they are weaker and their signal-to-noise ratio (S/N) is lower.

From autocorrelation of noise signatures (shown in the software manual), it is known that longer noise signatures have a better S/N in the autocorrelation at $t = 0$. It is therefore expected that from a S/N perspective more sources with a short noise signature duration would give similar results to fewer sources with a longer duration length. Figure 5 shows the retrieved reflections when short (maximum length $T_l = 5$ s) noise signatures are used, but with 8000 sources. Comparing this result with Figure 4f, based on 1000 sources, one can see that sufficiently many short-duration noise

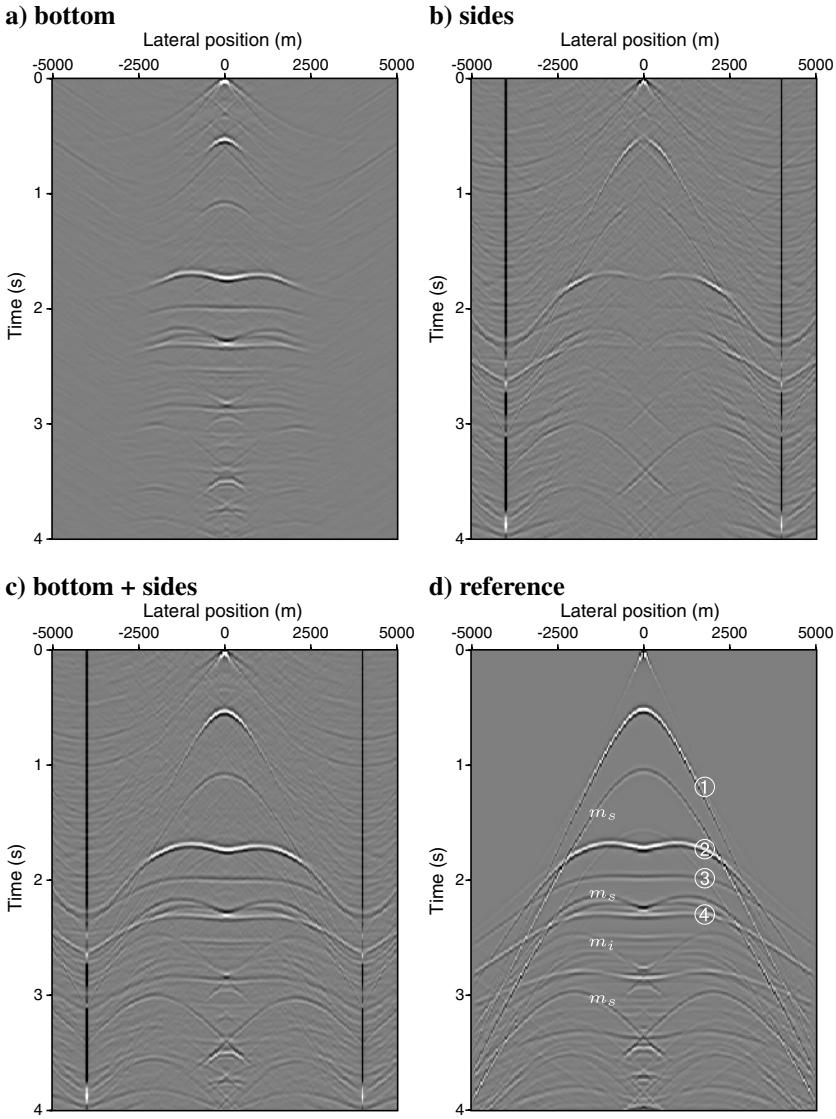

Figure 3. The retrieved reflection response for a virtual source placed in the middle of the model from Figure 2 at $x = 0$ m: (a) using only sources at depth level 3600 m; (b) using only the sides of the contour; (c) using all sources (creating a closed contour with the free-surface). (d) A directly modeled reference result for an actual source at $x = 0$ m. Note that outside the lateral extent of the contour ($|x| > 4000$) the retrieval is not correct. The left, right and bottom edges of the wavefields are tapered with a 450-m-long taper to suppress reflections from these sides. The numbers in the reference result (d) refer to the numbered reflectors in Figure 2, furthermore m_s indicate a surface multiple and m_i an internal multiple.

sources will eventually also retrieve the main reflection events, assuming the sources and the model are compliant with field ergodicity. One can interpret the many short noise signatures emitted by a number of closely situated sources as one long noise signature emitted from one (group) source. The long noise signature can then be thought of as consisting of bursts of short noise signatures originating from the direct surroundings of the single (group) source.

This would also mean that using longer passive measurements, more (short- and/or long-duration) passive sources are captured and a more complete retrieval can be obtained. In seismically active areas, a few days of recording might be sufficient, while for quieter areas of the earth several months might be needed.

In Figure 6 the average signature duration is kept constant (with an average length of 60 s), but the number of sources is varied. In the FD algorithm, the number of sources used to model one recording is set by one parameter `nsrc`). The only practical limit for the number of sources is the amount of available memory. The noise signatures for all sources are computed in advance and stored in memory. We can see that the more the randomly distributed sources, the better the retrieved result matches the reference result. Above a certain number of sources (in this example around 500), the strongest reflection events are retrieved correctly, meaning that the stationary-phase areas for those reflections are sampled densely enough. Adding more sources helps to retrieve other reflection information that has a narrower stationary region. For example, Figure 6a, constructed using 8000 sources, shows the bow-tie-shaped event starting at 3.0 s more completely than Figure 6b constructed when only 1000 sources were present.

Recording the contribution of more sources does not improve the S/N for the already correctly retrieved reflections. Figure 6f shows a

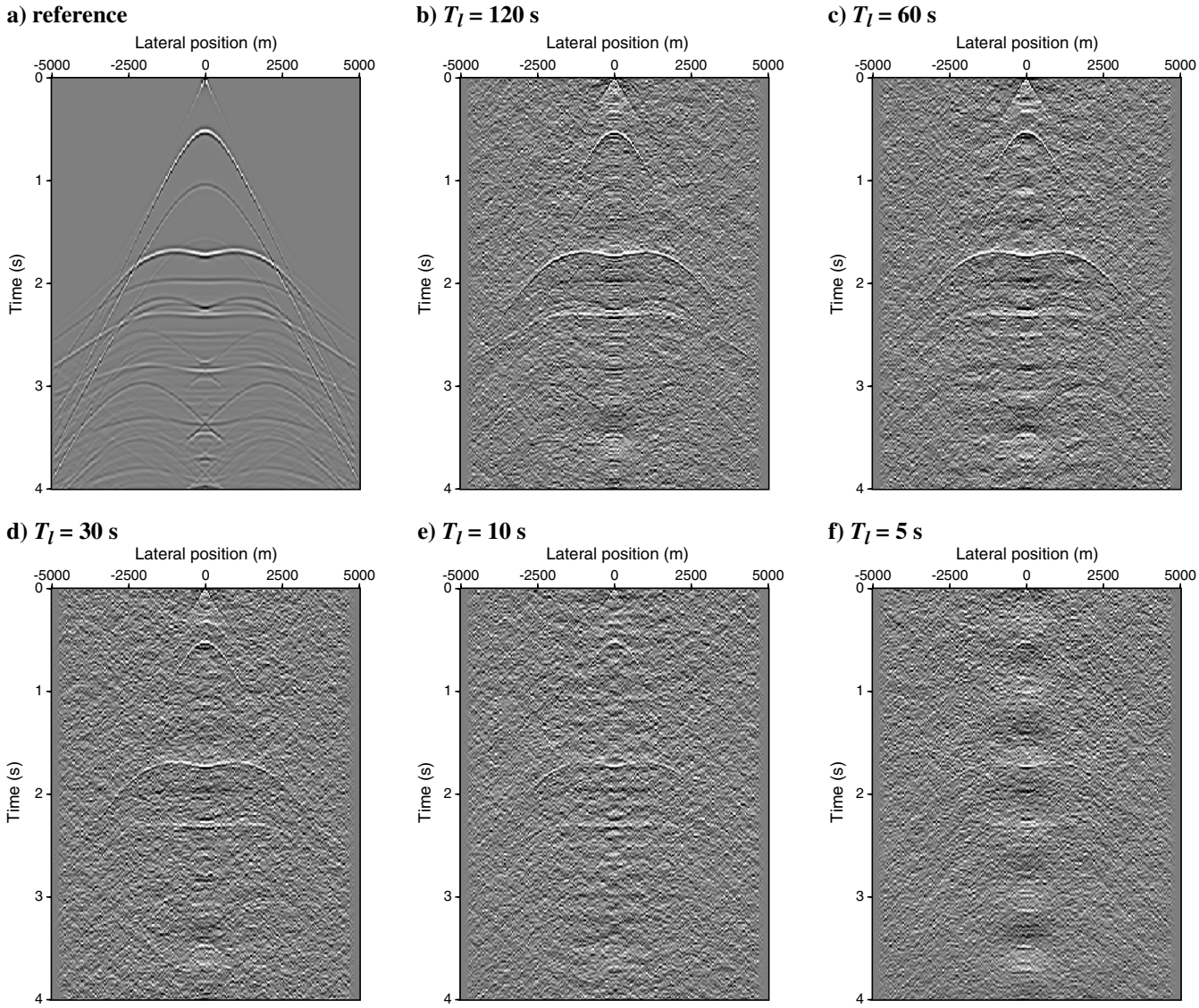

Figure 4. (a) A reference retrieved result (repeated from Figure 3d). Retrieved results using different maximum noise-source-signature lengths (T_l): (b) 120 s (c) 60 s (d) 30 s (e) 10 s, and (f) 5 s. To retrieve the seismic interferometry (SI) result we use noise signatures with a maximum frequency of 30 Hz, 1000 sources at random positions, a random start time of the noise sources between 0 and 120 s and a total recording time of 120 s.

comparison of the middle traces from the panels in Figure 6a–6e. The traces are normalized to the maximum value per trace (around $t = 1.75$). Note that the leftmost trace (using 8000 sources, from Figure 6a) has the most complete and correct reflection retrieval, but there is no S/N improvement compared to the trace based on only 50 sources (from Figure 6e). This is in contrast with NMO stacking, which improves the S/N by a factor $\sqrt{N}$, where N is the number of traces stacked. There are three possible explanations for the observed noise between the retrieved reflections. First, in our modeling example the sources are not placed on a surface, as is required by the theory, but are distributed in a volume below 500 m depth. Integration over this volume of sources will generate artifacts due to incomplete destructive interference. Second, the assumptions for smoothness of the medium parameters around the boundary are violated and these should also introduce artifacts. Third, the dipole sources at the source locations can not be replaced by scaled monopole sources because the normal on the surface does not coincide with the direction of the dipole source. On the other hand, even if the sources were nicely distributed along an ideal boundary surface $\partial\mathbb{D}_1$ and the Fresnel zone (Spetzler and Snieder, 2004) is sufficiently sampled by a certain number of sources (at least two sources per wavelength), adding more sources will not add extra information, since the constructive interference inside the Fresnel zone retrieves the physical amplitude.

In Figure 6, all the observed background noise is a result of the correlation, i.e., it is correlation noise. In field measurements, there is also random noise from the measurement equipment and this signal-to-random-noise level would improve when more sources are contributing to the retrieved reflections. It is expected that with the contribution of more sources this type of noise will decrease with $\sqrt{N}$, where N is the number of measured sources. The noise from the instrumentation, which is thought to consist of purely random signals, is not included in our modeling.

In the previous experiments we have varied the source length and number of sources, but not yet the active region of the sources. In Figure 7 the sources are placed between 2700 m and the bottom of the model by changing the parameters defining the source region. Comparing Figure 7 with Figure 4b one can see that the steeper dips (longer offsets) of the reflections are not retrieved when using only deeply placed sources. This is due to the fact that deep sources, also limited in lateral extent, are an approximation of the complete closed contour integral of equation 4. The missing parts of the contour are the vertical dashed lines in Figure 2 at $\pm$4000 m. If the lateral extent of the deeper sources is increased outside the receiver array, more higher angles of the reflections would be retrieved. Extending the lateral extent of the source means that the gridded model used in FD must be extended. The program `extendModel`, included in the software, can be used to extend the size of the gridded model in all directions. On the other hand, comparing Figure 7 and Figure 6b, we see that in the former even the later reflection arrivals are now visible, which means that the S/N of these arrivals is now higher. This can be explained by the fact that the source distribution for the results in Figure 7 now complies with the assumption of smooth media parameters around the source boundary and, consequently, less artifacts are generated.

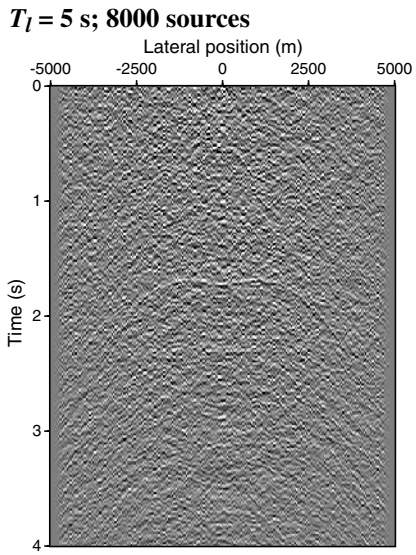

Figure 5. SI results using 8000 noise sources with a short noise signature duration of $T_l = 5$ s. The duration of the recording is 120 s. Compare this result with Figure 4f, which is based on 1000 sources and the same signature duration of $T_l = 5$ s.

Influence of source positions and signature

Figure 8 shows the recorded data for three different kinds of source distributions and two different source signatures. The source distributions are:

- random positions between $500 \le z \le 4100$ m (Figure 8a and 8d),
- random positions between $2700 \le z \le 4100$ m (Figure 8b and 8e),
- a horizontal line at $z = 2700$ m with regularly spaced sources, just below the deepest reflector (Figure 8c and 8f).

For the random source positions, 8000 sources are used. To simulate a plane wave at $z = 2700$ a source is placed on every grid point in the model (1001 sources) between -5000 and 5000 m at level $z = 2700$ and the sources become active simultaneously. The two types of source signatures are: a Ricker wavelet with a frequency peak at 10 Hz (with a maximum frequency of 30 Hz) and uncorrelated random source signatures (different for each source position) with a maximum frequency of 30 Hz.

The retrieved reflection responses of the recordings from Figure 8 are shown in the corresponding panels in Figure 9. The cleanest retrieval, i.e., the lowest level of correlation noise, is given by the plane-wave response with a Ricker wavelet as shown in Figure 9f, but this is also the poorest retrieval of reflection data. The correlation condition in equation 6 is not satisfied: Both the source signature and source position are strongly correlated. The retrieved reflections using uncorrelated noise signatures, but a correlated source depth position at the horizontal line $z = 2700$ is shown in Figure 9c. This retrieval is quite good and very similar to Figure 9b, where random source positions are used below $z = 2700$ m. From these three experiments, it can already be concluded that spatially uncorrelated source positions and uncorrelated time signals are important for a good quality of the retrieved reflections. Figure 9d and 9e use the same fixed (for all source positions) Ricker source signature, but have uncorrelated source positions. The retrieved reflection events are now clearly visible and the introduced noise is caused by incomplete destructive interference outside the Fresnel

zone and by the correlation between the source signatures. The latter is visible on the second reflector (at 1.2 s), which is better retrieved for the noise sources (compare with Figure 9a and 9b, respectively). Note that the results with the Ricker wavelet, using a random start time and source position, are in fact partly uncorrelated (in time) shot records because of the short signature of the Ricker wavelet. In general, as can be seen from equation 4, noninterfering impulse sources are required by SI. The randomness in the start time and source position in the experiment with the Ricker wavelets would ensure the noninterference condition for the earlier arrivals, but the later reflections and multiples would still be interfering with each other and thus their S/N would be lower.

The retrieval using noise signatures at random positions is shown in Figure 9a and 9b and similar reflection events and noise behavior are observed as in Figure 9c. A close examination of Figure 9a, where a volume of sources is used with $500 \leq z \leq 4100$ m, shows that higher angles are better retrieved compared with Figure 9b. However, there are also spurious events introduced (we indicate one event with an arrow).

In the examples of Figure 9a, 9b, 9d, and 9e the sources are originating from a volume. Using SI theory, based on a surface integral, these volume-distributed sources might not interfere destructively for all possible spurious reflections. As shown in Draganov et al. (2004) and Wapenaar and Fokkema (2006), when the medium below the sources is inhomogeneous, one will need a random distribution of sources to cancel the spurious events. The volume distribution of the sources between 500 and 4100 m cannot be considered as a smooth integration surface anymore. The result is that the normal to the surface will not coincide with the dipole

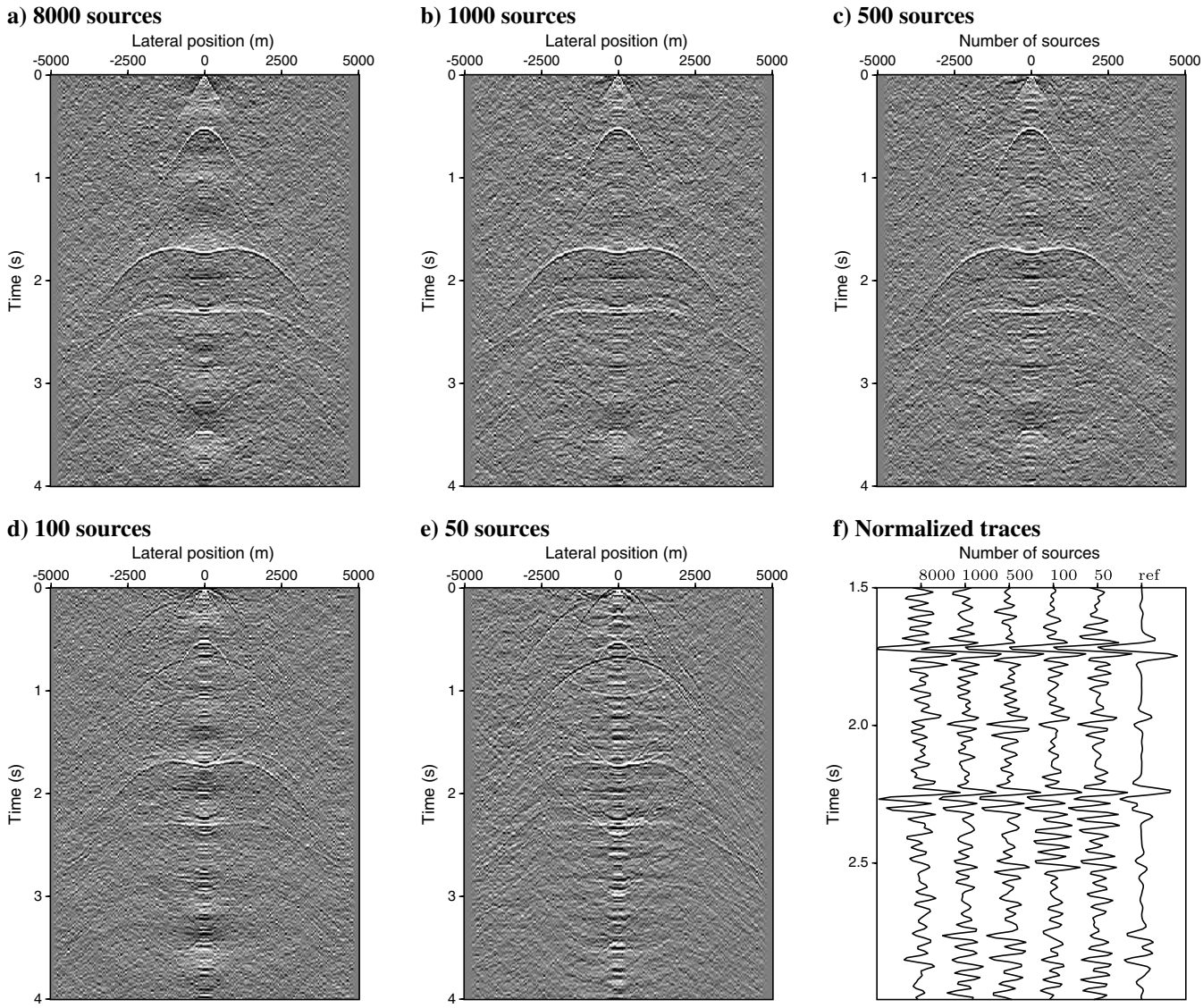

Figure 6. SI results for a varying number of sources. The sources have random positions in the model (represented by the black dots in Figure 2) below $z = 500$ m. The used noise signatures have a maximum frequency of 30 Hz, a length between 0 and 120 s, and start at a random time between 0 and 120 s. The average noise-source duration is 60 s and the total recording time is 120 s. The total number of the noise sources is (a) 8000, (b) 1000, (c) 500, (d) 100, and (e) 50. (f) A comparison of the normalized middle traces of the panels in (a) (first trace) until (e), respectively. The last trace in (f) is the reference result.

source radiation pattern and the assumptions made for SI equation 4 (approximate dipoles by scaled monopoles) are not satisfied anymore. Another assumption for the derivation of relation 4 that is violated is the one about the smoothness of the medium parameters around the source surface. The above two violations would result in the spurious events in Figure 9a and 9d. Note that the sources for the results in Figure 9b and 9e are distributed in one layer, that is, the medium there is smooth. Furthermore, the concentration of sources in the latter case is a better approximation of a smooth boundary.

Influence of attenuation and source-strength

The above-described theory is strictly valid for media without intrinsic losses. When SI equation 4 is applied in dissipative media, spurious events will show up in the retrieved data (see Draganov et al. [2010]). To investigate this, the viscoacoustic scheme of the program is used on the same gridded model, but now with an overall constant quality factor $Q_p = 15$. Modeling dispersion in the FD compute kernel is implemented by adding extra terms to introduce losses in the pressure field (see section three of the manual for implementation details). Figure 10a shows the directly modeled reflection response. Comparing this picture with the result in Figure 10b, obtained with randomly distributed sources below $z = 2700$ m, we see that a spurious event is visible (around 0.3 s). This distribution of sources can be interpreted as (delayed) sources located on a flat surface below the deepest reflector. For the same source distribution, but without losses (see Figure 9b) there was no spurious event at that arrival time. In Figure 10c the sources are placed throughout the whole model and the summation of all those sources can be seen as a volume integral. In that case the theory predicts (Snieder, 2007) that a correct retrieval, without spurious events, could be obtained again. Although our implementation of the source volume is not fully compliant with that theory, which requires the volume distribution of the sources to be proportional to the intrinsic losses, in Figure 10c we already observe that the spurious event around 0.3 s has been significantly weakened.

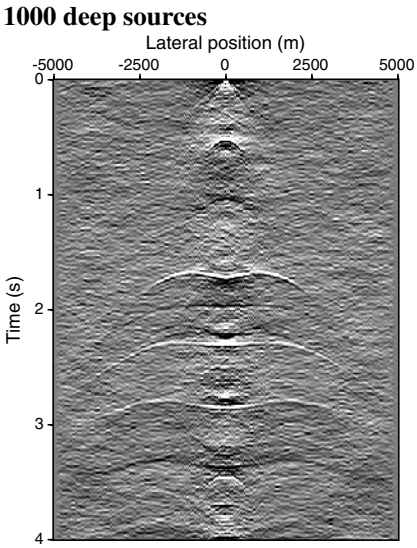

Figure 7. Interferometry results obtained using 1000 sources positioned below the deepest reflector in the model ($z \geq 2700$). The random sources have a maximum source duration of 120 s.

To test our interferometry algorithms for field-recorded data, a long recoding time of 3600 s is simulated. During this simulation time the FD program activates 1500 sources, all with the same source strength, located below $z = 2700$ m. The sources have random starting times between zero and 3600 s, and a maximum source duration of 500 s (average 250 s). The interferometry results are shown in Figure 11 for three different combinations of correlations. In the frequency domain these correlations are represented as

$$\hat{C} = \hat{A}^* \hat{B}, \tag{8}$$

$$\hat{C} = \hat{B} \hat{A}^*, \tag{9}$$

$$\hat{C} = \hat{A}^* \hat{B} + \hat{A} \hat{B}^*. \tag{10}$$

From a computational point of view correlation equation 10 is the most efficient one because it only computes the real part. However, which correlation will give the best retrieval is difficult to predict beforehand, as it depends on the actual position of the passive sources and the subsurface inhomogeneities, and we advise calculating both terms, i.e., both the causal (equation 8) and a-causal (equation 9). The program `fconv`, in the `utils` directory of the software, can be used to compute the three different correlations.

In field passive measurements, recordings will be written to a file at regular times to empty the buffers of the recording device. During the FD modeling, we have simulated this by writing the recorded traces to a unique file every time 16,384 samples (with time-sampling interval of 8 ms) were modeled. The parameter `rec_ntsam` sets the maximum number of samples in the output files. If this number is exceeded, a new (sequentially numbered) file is opened to write the results. This results in 28 files where the last sample in a file connects, without losing a sample, to the first sample of the next file. These modeling results can then be used to verify correlation algorithms. In our correlation program and given a fixed (short) output length, the correlation is carried out continuously over the full recording time (3600 s) (Thorbecke and Drijkoningen, 2007).

Figure 12b shows the same experiment as in Figure 11a, but now the strengths of the 1500 sources are varying in amplitude with a variation as shown in Figure 12a. The amplitude variations are implemented as a (random) scale factor applied to the precomputed source signatures. The correlation result is still good and only minor changes are visible when compared to Figure 11a. To compensate for the amplitude differences, the measured signals are normalized per trace (divided by the root mean square value; for another technique the reader is referred to Curtis and Halliday [2010]). The retrieved reflection response with normalized traces is shown in Figure 12c. Due to the many sources (1500) and the long source signature of 500 s, the amplitude differences between the sources are not clearly distinguishable in the SI result and differences are averaged out.

With the results in Figure 13, the effect of the source strength is investigated further in a more extreme case, as now we use 150 sources with a maximum signature duration of 120 s. Figure 13a shows a reference result without any amplitude variation between the sources. To construct Figure 13b, a Gaussian distribution was used, while for Figure 13c a flat distribution was used. The amplitude range between the weakest and strongest source is 25,000.

The SI result in Figure 13c exhibits strong amplitude contributions that dominate the retrieved events and consequently one cannot interpret in it retrieved reflections. On the other hand, the result in Figure 13b clearly shows retrieved reflections. This means that when the noise sources have varying amplitudes, in addition to the random distribution in time and space, also the amplitude distribution should be random. For more realistic modeling experiments, a good statistical model should be implemented in the code representing the amplitude variation occurring in seismically active areas.

Receivers on topography

To make an even more complicated model, a free surface with topography has been included and furthermore the subsurface has been modified to contain nonhorizontal structures (see Figure 14). To place the receivers on the topography, a special trick is used. The receivers are defined on a horizontal plane above the topography ($z = -800$ m). The layer above the topography is then defined to have P-wave velocity of 0 m/s. In the program, the receivers are sunk in depth through this zero-velocity layer until they encounter a nonzero velocity value. These are the grid point the receivers are placed on. We choose this model because in rough-terrain areas it is often difficult to use active sources for seismic surveys. In such areas, passive seismics could be a solution since only receivers have to be placed (together with a storage device to save all the measurements made for a long period of time).

To simulate passive sources, 1500 sources have been placed around a section of dipping layers that we model as seismically active. In Figure 14, the sources are shown as black dots. The

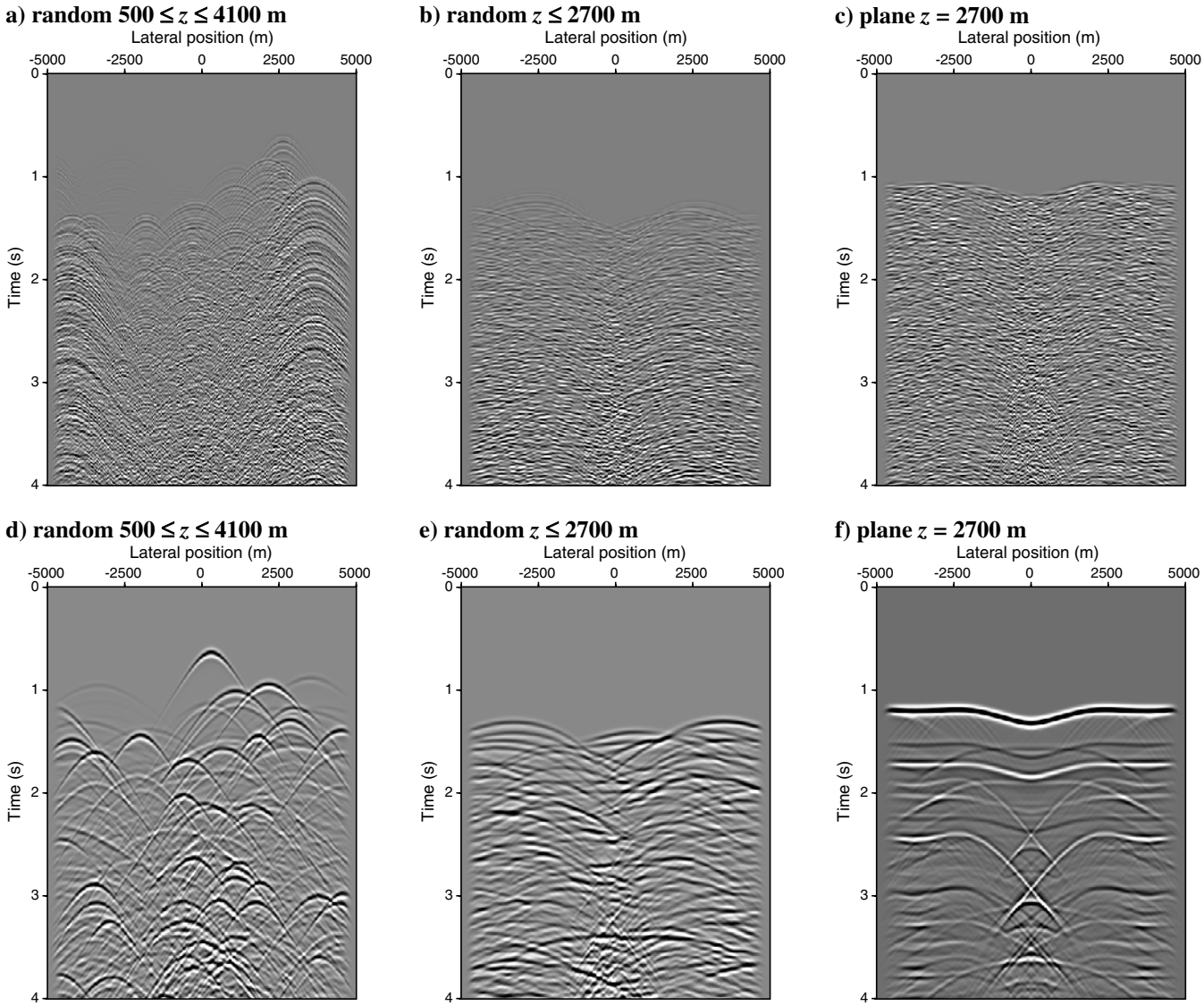

Figure 8. The first four seconds of modeled recordings at the surface that are used as the input for SI. The subsurface sources are distributed along x-positions between −5000 and +5000. The z-range of the sources is indicated in the text below each of the pictures. Noise signatures (every source has a unique signature) are used in (a), (b), and (c) and the same Ricker wavelet is used in (d), (e), and (f). The sources in (c) and (f) are started simultaneously.

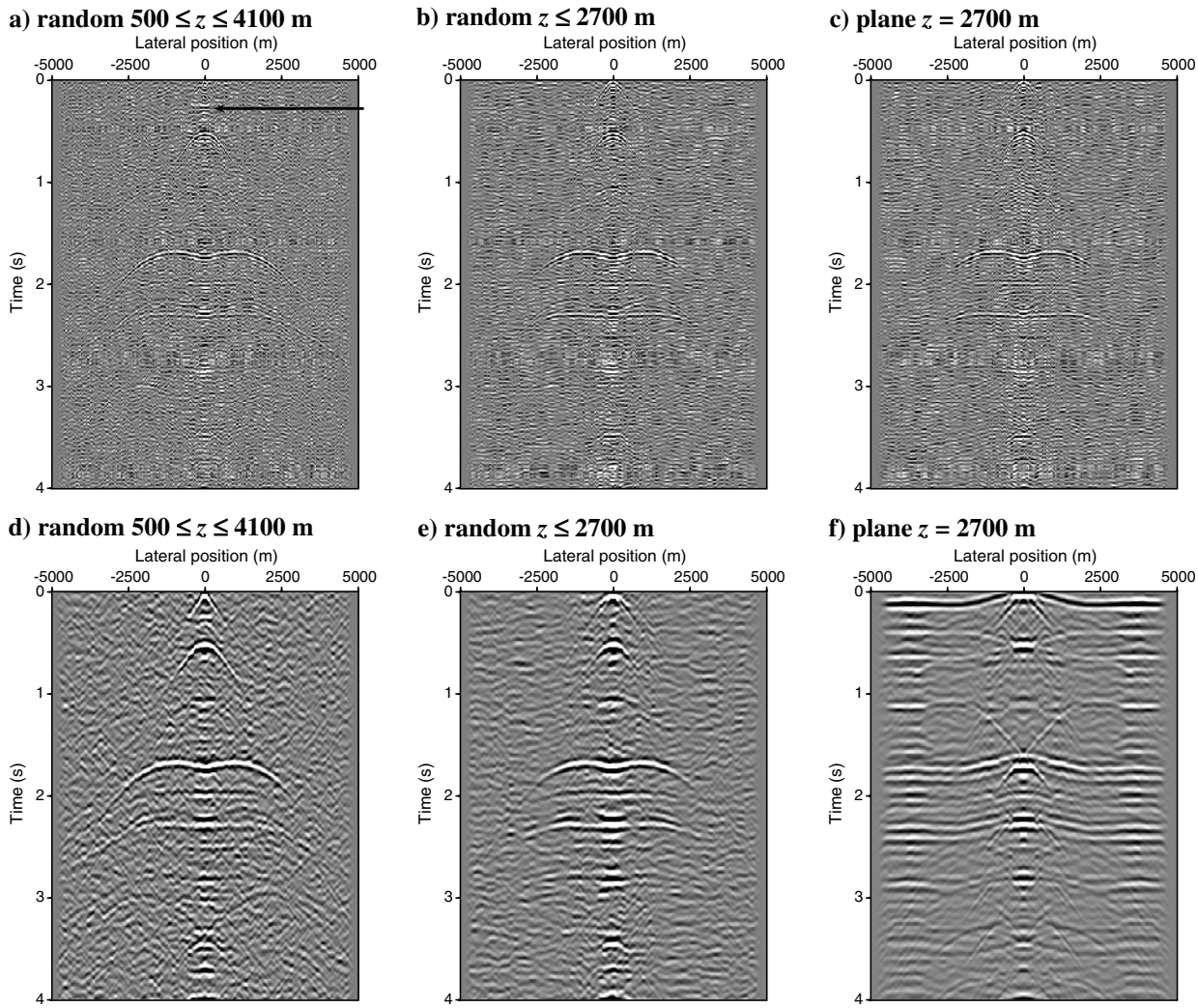

Figure 9. Retrieved results from the application of SI when the inputs are recorded signals as shown in the corresponding panels in Figure 8. The arrow indicates a spurious event introduced by the type of source distribution.

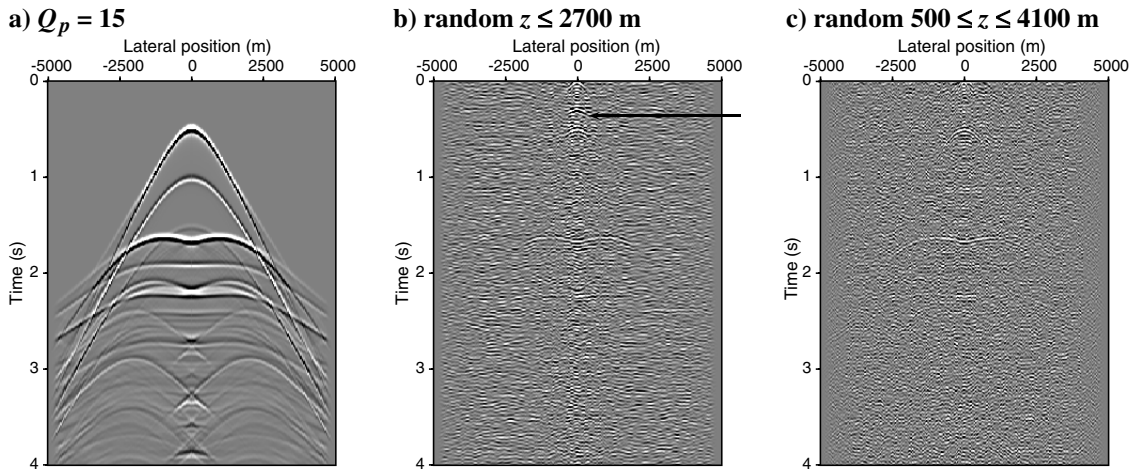

Figure 10. Reflection results in viscoacoustic media with constant quality factor $Q_p = 15$; (a) the directly modeled result; (b) and (c) show the SI results for two source distributions as indicated in the text below the panels.

average source length is 25 s and a random signature is used with a maximum frequency of 30 Hz. The modeling time is 3600 s.

A directly modeled result, generated with an active source in the middle of the model on the free-surface, is shown in Figure 15a. The retrieved reflection data in Figure 15b confirm that with the chosen source configuration an accurate retrieval of the reflection events is possible. Note that the later reflection arrivals are buried inside the correlation noise. As discussed above, longer recording times would bring forward these weaker arrivals as well.

DISCUSSION

Draganov et al. (2004) show the effect of clustered noise sources on the result of SI. Their result is closely connected to the influence of the strength of the sources. In Figure 12 and 13, we showed the retrieved results when the source strength varies randomly. When the source strength variation exhibits a flat distribution (Figure 13c), then the retrieved results are wrong, as only the strongest sources contribute to the final result.

More numerical modeling examples are needed to formulate general statements as to what influences the quality of retrieved reflections. The `FiguresPaper` directory contains extra scripts for investigating the dependence of the retrieved results from the modeled data as used for Figure 6 and Figure 7 on fixed signature length and maximum frequency content. The reader is invited to draw his own conclusions from running these scripts.

From our numerical experiments, we argue that spurious events and noise introduced by the correlation will always be visible, no

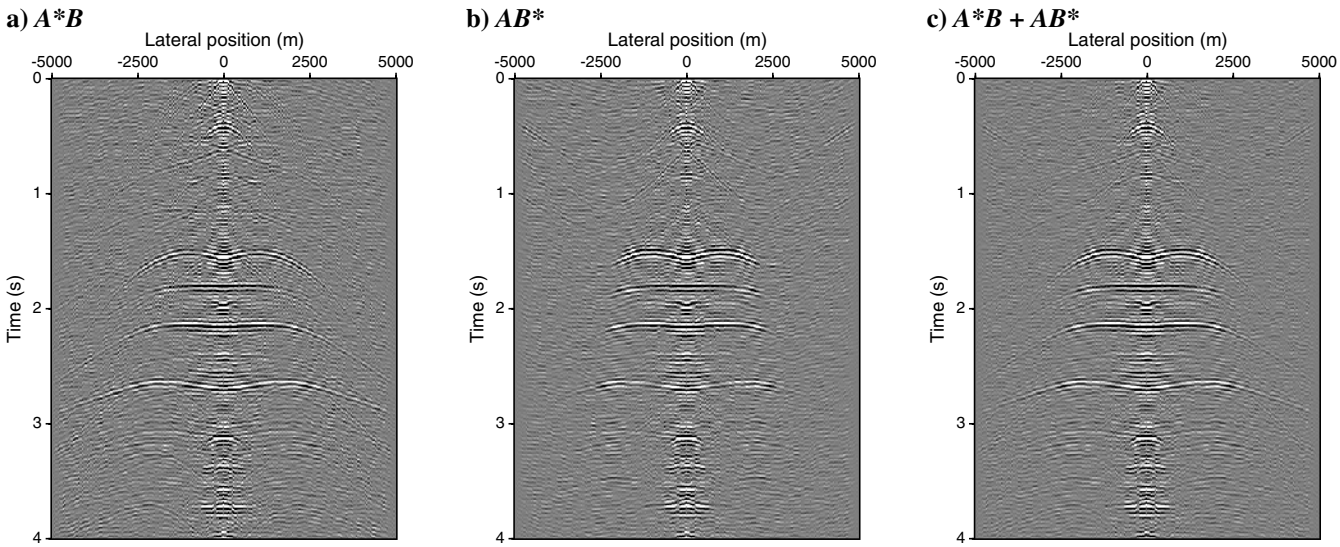

Figure 11. SI retrieval with long signals (maximum duration 500 s) and long recording times (3600 s). Panels (a), (b), and (c) show three different correlation implementations as indicated below the panels.

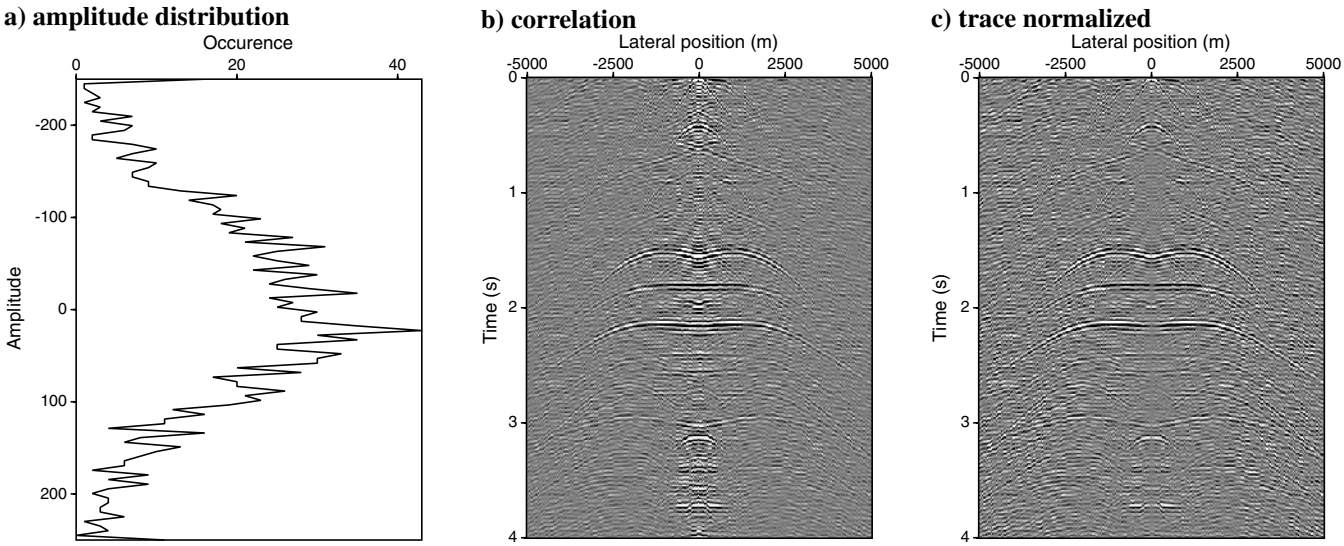

Figure 12. SI with amplitude variations in the source strength. The (Gaussian) distribution of in total 1500 source strengths is given in (a), the correlation result in (b), and a correlation result for (energy) normalized traces in (c).

matter how long the recordings will be. This is because, in reality, the assumptions for SI are not fulfilled and violating these will introduce noise and/or spurious events.

Before one starts modeling realistic experiments, it must first be investigated what kind of sources distributions and signature lengths are geologically expected. More research is also needed to investigate the radiation pattern of passive sources and retrieval of source characteristics by crosscorrrelation. Mathematical derivations and approximations based on that knowledge can then be made. For example, when a source distribution does not satisfy the assumptions underlying equation 6, the spatial delta function becomes a geologically constrained spatial function.

In the previous sections, we saw that spurious events might arise due to intrinsic losses in the medium. Spurious events might also

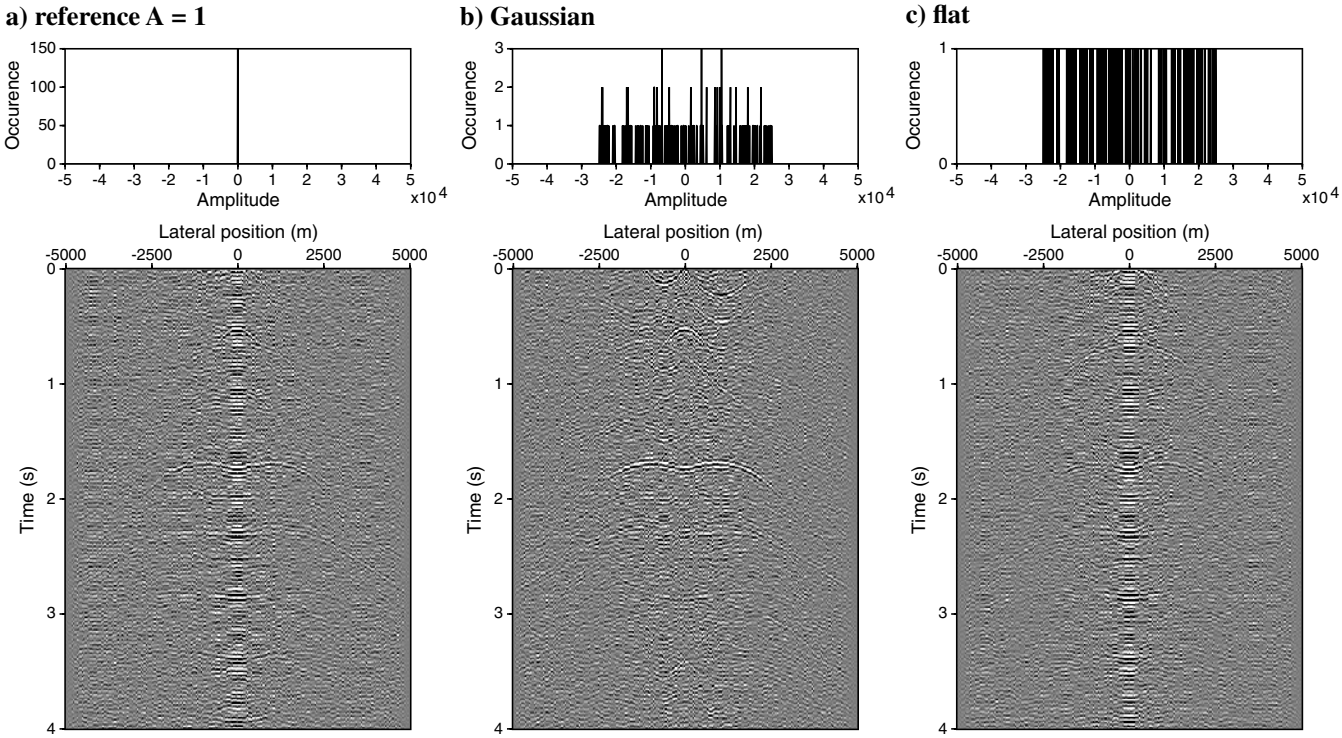

Figure 13. SI with amplitude variations in the source strength. The amplitude changes, of in total 150 sources, are varied from 0 to ±25000. The result without amplitude variations is shown in (a), (b) shows the correlation result using a Gaussian amplitude distribution, and (c) flat distribution. Note that the amplitude used to construct panel (a) is one for all sources.

Figure 14. A more complicated model where 1500 passive sources are active in the area between depth levels 1750 m and 2600 m and are visible as black dots within the model. The receivers are placed from −5000 m to 5000 m at every 20 m on the topography.

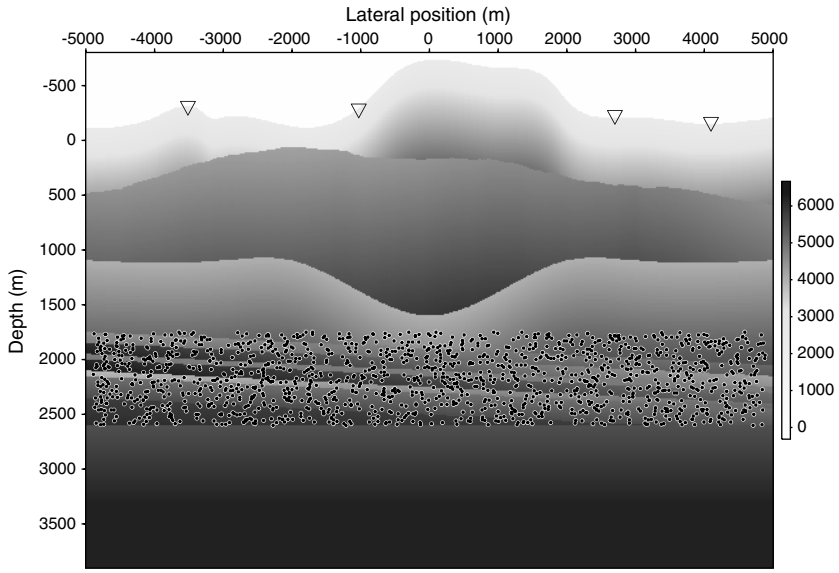

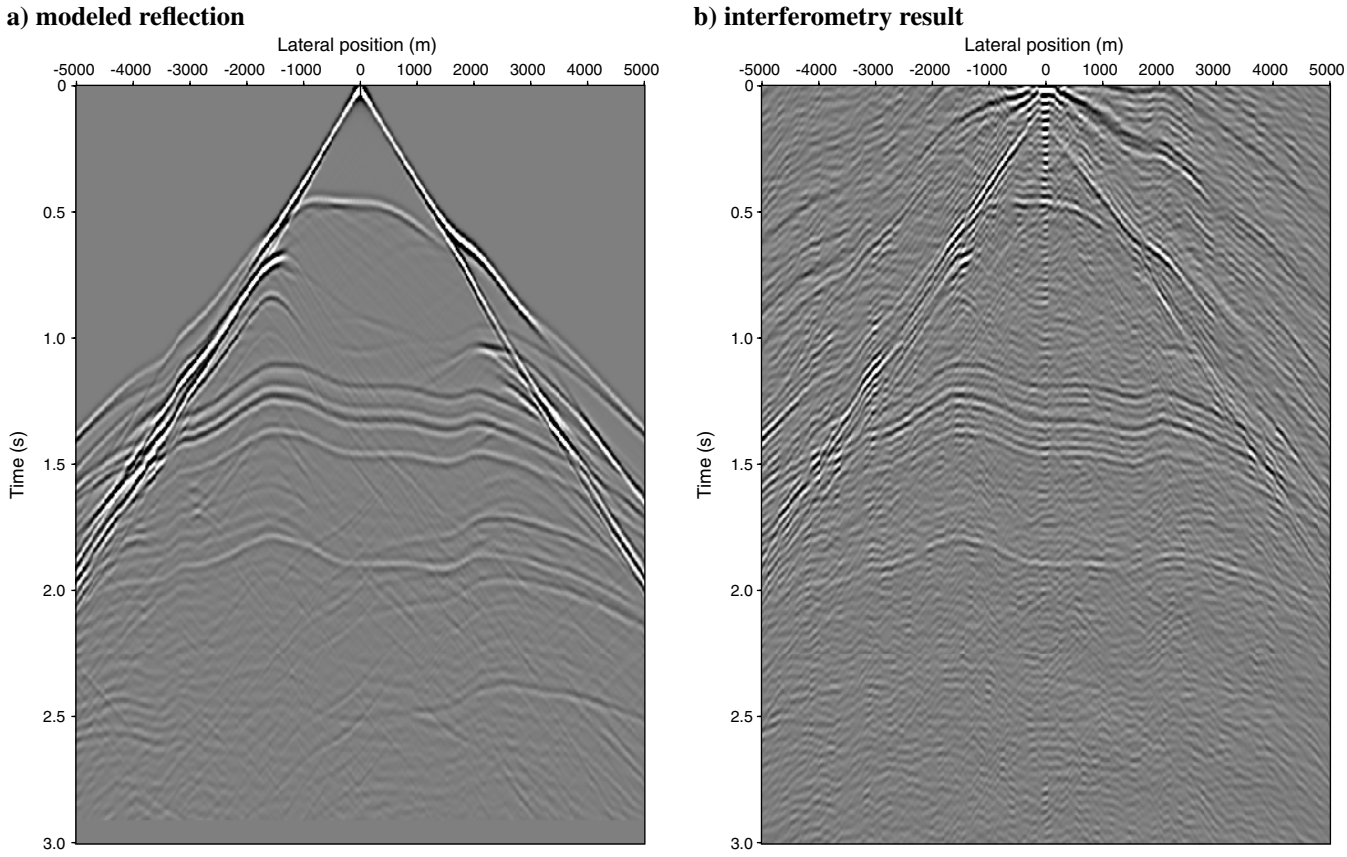

Figure 15. (a) The modeled reflection response for a source at 5000 m placed on the topography. (b) The interferometry result using the sources indicated in Figure 14.

arise in the case of so-called one-sided illumination, that is when the source boundary does not completely enclose the receivers (Snieder et al., 2006; Thorbecke and Wapenaar, 2008). These spurious events could also be investigated with the FD code, for example by not using a free surface. When intrinsic attenuation is present in the medium, one could use single-channel deconvolution to account for the losses (Snieder et al., 2009). When illumination issues are present, one could try to balance the amplitudes as proposed by Curtis and Halliday (2010). Both above-mentioned types of spurious events, as well as problems that might arise due to varying source amplitude strength, could be remedied using SI by multidimensional deconvolution (Wapenaar et al., 2008a, 2008b; van der Neut et al., 2009).

The software enables the modeling of many sources simultaneously and could therefore also be used for experiments with blended sources.

The limitations and (im)possibilities of a FD program, together with a detailed explanation of how to use the parameters and certain specific implementation issues a user must be aware of, are to be found in the software manual. More specific limitations related to the modeling for SI are that the dipole-source direction is always oriented along one of the axis of the cartesian grid, and that modeling of traction sources is not yet implemented.

We hope that by making the modeling software freely available, other groups can also benefit from our efforts and use the software to gain more insight in the practical issues of SI, and even implement new functions into the code.

CONCLUSIONS

We use a finite-difference modeling code to investigate the dependence of the retrieved reflection response by SI on different characteristics of noise sources present in the subsurface. The program was specially developed to facilitate such tests and gives the possibility to model the response from many noise sources, simultaneously active and/or partly overlapping in time, in one run of the program. Even though the study is limited in terms of the definitive quantitative conclusions that can be drawn from it, the results are illustrative and can be used to draw the following qualitative conclusions. When the noise sources are correlated both in time and space, the retrieved reflection response is wrong. When the sources are of short duration and thus correlated, in the limiting case transients with the same wavelet, uncorrelated starting time and locations still result in the retrieval of the correct reflection response. If the sources are instead correlated in space by lying at the same depth level, but uncorrelated in time, the reflection response is again retrieved. We also showed that the longer the time duration of the signals, the better the retrieved result. The effect of the short duration of the noise signals would be remedied by recording the response of more noise sources. When a reflection event is retrieved with a good quality, that is, its

stationary-phase region is sampled by at least two sources, the addition of more sources does not improve the retrieval S/N of this reflection; it only increases the S/N of reflections that were insufficiently retrieved. When intrinsic losses are present in the medium, noise sources, which are randomly distributed inside the complete volume, can suppress nonphysical arrivals that arise due to the losses. We also investigated the influence of the strength of the sources on the retrieved results. We showed that as long as the amplitude-variation distribution of the noise sources is random, one can retrieve the reflection response using SI even in the extreme case of the amplitudes varying over several orders of magnitude.

ACKNOWLEDGMENTS

We thank Statoil for their financial support of this research. Specifically, Gerrit Toxopeus is thanked for fruitful discussions about the modeling results and suggestions for new experiments. The authors would like to thank the associate editor Joe Dellinger, the reviewers Ivan Vasconcelos, Sjoerd de Ridder, and three anonymous reviewer for their constructive suggestions and comments and the thorough testing of the software.

APPENDIX A

ALGORITHM AND IMPLEMENTATION

To simulate passive seismic measurements we have chosen to use a 2D FD approach based on the work of Virieux (1986) and Robertsson et al. (1994). The main reason for choosing the FD method is that it runs well on standard X86 and multicore hardware (including graphical cards) and is easy to implement. For the moment, only the 2D case is implemented to gain experience and to be able to run many experiments within a short computation time. For reading input parameters and access files on disk, use is made of the Seismic Unix (http://www.cwp.mines.edu/cwpcodes/SU) parameter interface and SU-segy header format with local IEEE floating point representation for the data. Four different schemes are implemented: acoustic, viscoacoustic, elastic, and viscoelastic. We will not go into all the implementation details and only explain the specific aspects related to the modeling of measurements that can be used to study SI. The main difference with other FD codes is the possibility to use band-limited noise signatures positioned at random source positions in the subsurface and model the combined effect of all those sources in only one modeling step. Existing modeling codes are able to model the same result, but are less efficient or

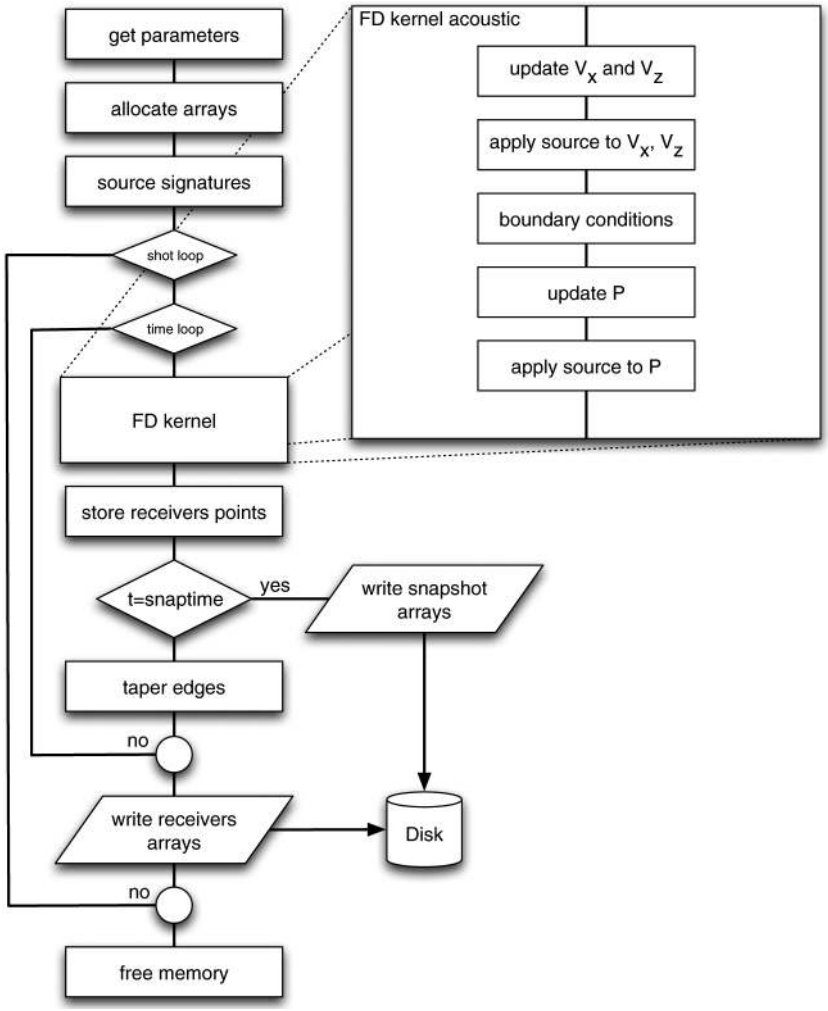

Figure A-1. Flow chart of the FD algorithm. The FD kernel of the acoustic scheme is explained in the inset in more detail. The two decision loops are for the number of shot positions and the number of time steps to be modeled. In the chart, t represents time, V_x and V_z the horizontal and vertical particle velocity, respectively, and P the acoustic pressure.

less user friendly (more than one program is required to do the modeling of all the passive sources). More details about the used algorithm and the options within the program can be found in the manual distributed with the code. In this appendix, we explain the flow of the algorithm and more specifically the implementation of the noise signatures. In the last part of the appendix, the acoustic FD result is verified with four analytical Greens functions in a 2D homogeneous acoustic medium.

Finite-difference algorithm

Following the flow chart of Figure A-1 we explain the algorithm step by step. The program starts by reading in the given parameters and together with default values sets up a modeling experiment. The velocity and density models are read in together with the grid spacing. Using the model grid spacing and the defined time sampling, a check is made for the stability and dispersion criteria. The random source positions and signature lengths are computed and all arrays are allocated. The source signatures are calculated in advance and we explain this in more detail in the next part.

The algorithm contains two loops: the outer loop is for the number of shots and the inner loop for the number of time steps to be modeled. For SI modeling with random source positions, the number of shots in the outer loop is set to one, all sources will become active within the inner time loop. Every time step, the FD kernel is called to update the wavefields and inject source amplitudes, followed by storing of wavefield components on the defined receiver positions and, if requested, a snapshot of the wavefield components is written to disk. The last task within one time step is suppressing reflections from the sides of the model by tapering the edges of the wavefields with an exponentially decaying function. After all time steps are calculated, the stored wavefield components at the receiver positions are written to disk.

In the inset in Figure A-1 the acoustic FD kernel is sketched in more detail. Inside the kernel, the particle-velocity fields V_x and V_z are updated first. If there are sources active on the particle-velocity fields, these source amplitudes are added to the V_x and V_z fields after the update. This is done for all the defined source positions. The pressure field P is updated next and pressure-source amplitudes are added to the updated pressure field. This last step completes the FD kernel.

Modeling noise signatures

The (random) position of the sources can be implemented straightforwardly on the cartesian grid of the FD program. The

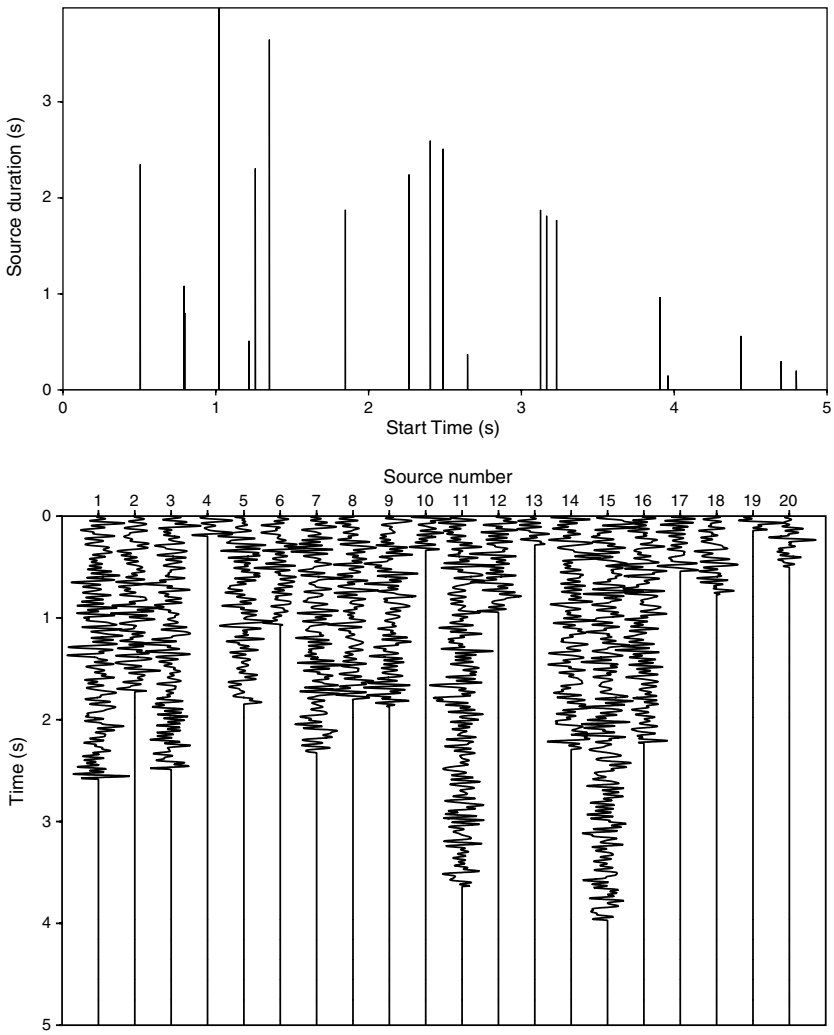

Figure A-2. Random source signatures with varying source duration (bottom). The sources become active at a precalculated random time within the total modeling time (top).

generation of a random (uncorrelated) signal requires more attention. Unless mentioned differently, the probability density of the random functions (to generate the source positions and noise signals) has a uniform distribution.

The noise signals are created by assigning, in the frequency domain, random values (between −0.5 and 0.5) to the real and imaginary part of the source signal for each frequency up to a given maximum frequency. This signal is transformed back to the time domain and truncated in time to the desired source duration. Figure A-2 shows in the time domain 20 random signals with an average duration of 2.5 seconds. Truncation in the time domain will introduce high frequencies in the spectrum above the predefined maximum and can give rise to dispersion effects during the FD modeling. To suppress these high frequencies, the beginning and the end of the source signals are smoothly extrapolated (using cubic splines) to an amplitude value of 0.0. The bottom pictures in Figure A-3 show a noise signal and its amplitude spectrum. This signal was constructed with a maximum frequency of 30 Hz. The start and end of the noise signal are smoothly beginning and finishing at amplitude 0.0 as shown in the zoomed top pictures of Figure A-3. Despite the smooth start and end of the signal, the spectrum of the noise signal does continue after 30 Hz, but the amplitude after 30 Hz is so low that it does not give rise to noticeable dispersion in the modeling. As an option, the calculated noise-source signatures can be written to a file for further inspection.

Verification of the numerical results

To verify the accuracy and the correctness of the FD program we have compared the FD calculation of a Green's function in a homogenous acoustic medium with the analytical Green's functions. Four analytical Green's functions are used for verification:

- monopole source and pressure (P) receivers,
- monopole source and vertical particle-velocity (V_z) receivers,
- dipole source and P receivers,
- dipole source and V_z receivers.

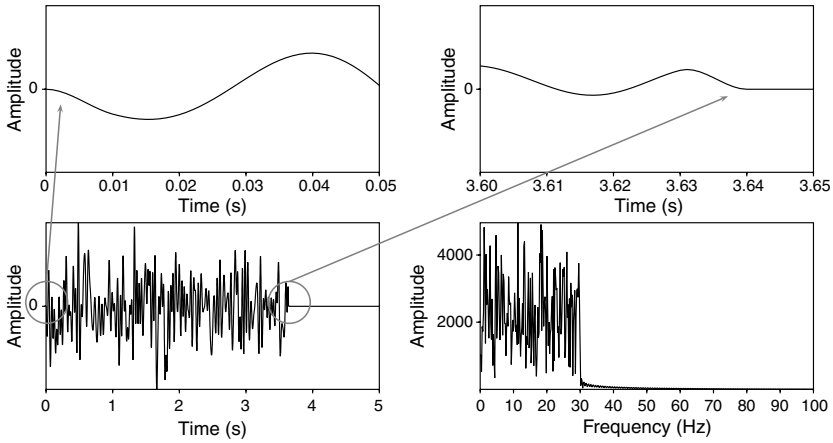

Figure A-3. Random source signature and its amplitude spectrum (bottom left and right, respectively). The start and end of the source-signature are smoothly (by means of a 10-point cubic spline extrapolation) beginning from and finishing at amplitude 0.0. This smooth transition zone limits the amount of energy in the frequency spectrum after the defined maximum frequency. (top) Zoomed in start and end of the signal.

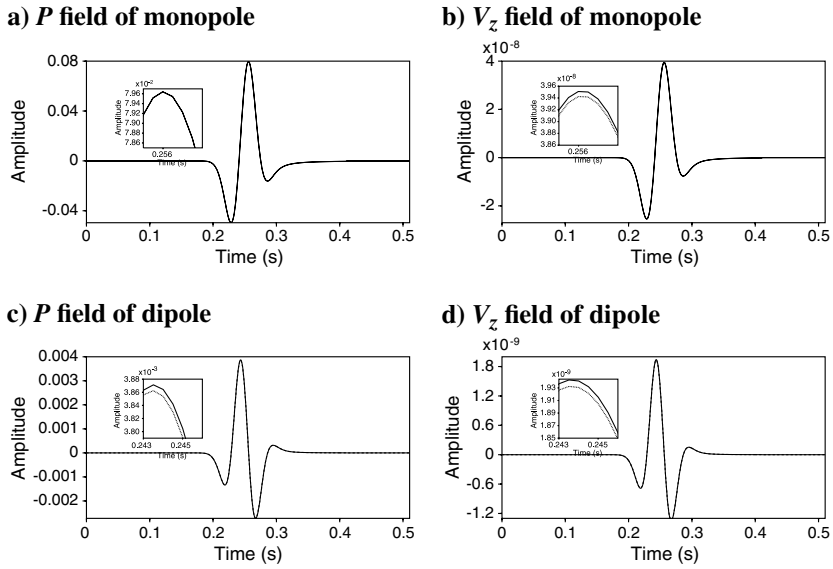

Figure A-4. Comparison of Green's functions in an acoustic homogeneous medium for monopole (top) and dipole sources (bottom) with pressure (P) and particle velocity (V_z), left and right, respectively. The insets show the differences for the positive peak of the wavelet, the lower dotted line represents the FD result.

The corresponding analytical Green's functions are given by:

$$P^{\text{mon}} = \frac{-j}{2} H_0^{(2)}(kr), \tag{A-1}$$

$$V_z^{\text{mon}} = \frac{\cos(\phi)}{2\rho c} H_1^{(2)}(kr), \tag{A-2}$$

$$P^{\text{dip}} = \frac{-jk}{2} \cos(\phi) H_1^{(2)}(kr), \tag{A-3}$$

$$V_z^{\text{dip}} = \frac{k\cos^2(\phi)}{2\rho c} H_0^{(2)}(kr) + \frac{k(1-2\cos^2(\phi))}{2\rho c kr} H_1^{(2)}(kr), \tag{A-4}$$

where

$$H_0^{(2)}(kr) = J_0(kr) - jY_0(kr), \tag{A-5}$$

$$H_1^{(2)}(kr) = J_1(kr) - jY_1(kr), \tag{A-6}$$

$$r = \sqrt{(x^2 + (z_s - z_r)^2)}, \tag{A-7}$$

$$\cos(\phi) = \frac{|z_s - z_r|}{r}, \tag{A-8}$$

x represents the lateral distance and z_s and z_r are the depth positions of the source and receiver, respectively. The Bessel functions of the first kind of orders zero and one are J_0 and J_1, respectively. The Bessel functions of the second kind of orders zero and one are Y_0 and Y_1, respectively. The wavenumber $k = \omega/c$, where c is the velocity of the medium. The analytical responses are generated by the program "green," included in the `utils` directory of the source code.

In the staggered-grid implementation, the P- and V_z-fields are positioned at different spatial grids and the V_z fields have been interpolated to the P-field grid position to be able to compare them with the analytical solution positioned at the P-field position. The FD scheme is also staggered in time and the modeled P-field is shifted half a time step compared to the V_z-field. For the implementation of a dipole source, two grid positions are used and this gives an extra time delay of $\frac{0.5\Delta z}{c}$, where c is the velocity at the source position and Δz the discretization step in the z-direction. In the comparison with the analytical Green's functions these discretization effects have all been taken into account.

The comparison between the analytical Green's functions and the FD computed results are shown in Figure A-4 for the four different configurations mentioned. The curves are perfectly overlapping and only after zooming in at the peak of the wavelet it is possible to observe differences. The difference between the analytical Green's function and the FD results is less then 1% of the peak of the analytical Green's function.

The reference medium has a velocity of 2000 m/s and a density of 1000 kg/m^3. The source is positioned 500 m below the receiver. For the FD code, a spatial grid of 2.5 m and a time step of 0.5 ms has been used to compute the results.

REFERENCES

Bakulin, A., and R. Calvert, 2004, Virtual source: New method for imaging and 4D below complex overburden: 74th Annual International Meeting, SEG, Expanded Abstracts, 2477–2480.

Bakulin, A., and R. Calvert, 2006, The virtual source method: Theory and case study: Geophysics, **71**, no. 4, SI139–SI150. doi: 10.1190/1.2216190.

Bojarski, N. N., 1983, Generalized reaction principles and reciprocity theorems for the wave equations, and the relationship between the time-advanced and time-retarded fields: Journal of the Acoustical Society of America, **74**, 281–285, doi: 10.1121/1.389721.

Campillo, M., and A. Paul, 2003, Long-range correlations in the diffuse seismic coda: Science, **299**, 547–549, doi: 10.1126/science.1078551.

Curtis, A., and D. Halliday, 2010, Directional balancing for seismic and general wavefield interferometry: Geophysics, **75**, no. 1, SA1–SA14, doi: 10.1190/1.3298736.

Draganov, D., X. Campman, J. Thorbecke, A. Verdel, and K. Wapenaar, 2009, Reflection images from ambient seismic noise: Geophysics, **74**, no. 5, A63–A67, doi: 10.1190/1.3193529.

Draganov, D., R. Ghose, E. Ruigrok, J. Thorbecke, and K. Wapenaar, 2010, Seismic interferometry, intrinsic losses and Q-estimation: Geophysical Prospecting, **58**, 361–373, doi: 10.1111/(ISSN)1365-2478.

Draganov, D., K. Wapenaar, W. Mulder, J. Singer, and A. Verdel, 2007, Retrieval of reflections from seismic background-noise measurements: Geophysical Research Letters, **34**, L04305–1-4, doi: 10.1029/2006GL028735.

Draganov, D., K. Wapenaar, and J. Thorbecke, 2004, Passive seismic imaging in the presence of white noise sources: The Leading Edge, **23**, 889–892, doi: 10.1190/1.1803498.

Ramírez, A. C., and A. B. Weglein, 2009, Greens theorem as a comprehensive framework for data reconstruction, regularization, wavefield separation, seismic interferometry, and wavelet estimation: A tutorial: Geophysics, **74**, no. 6, W35–W62, doi: 10.1190/1.3237118.

Rayleigh, J. W. S., 1878, The theory of sound: Dover Publications, Inc., volume **II** (Reprint 1945).

Rickett, J., and J. Claerbout, 1999, Acoustic daylight imaging via spectral factorization: Helioseismology and reservoir monitoring: The Leading Edge, **18**, 957–960, doi: 10.1190/1.1438420.

Robertsson, J. O. A., J. O. Blanch, and W. W. Symes, 1994, Viscoelastic finite-difference modeling: Geophysics, **59**, 1444–1456, doi: 10.1190/1.1443701.

Schuster, G. T., J. Yu, J. Sheng, and J. Rickett, 2004, Interferometric/daylight seismic imaging: Geophysical Journal International, **157**, 838–852, doi: 10.1111/gji.2004.157.issue-2.

Shapiro, N. M., and M. Campillo, 2004, Emergence of broad- band rayleigh waves from correlations of the ambient seismic noise: Geophysical Research Letters, **31**, L07614–1-5, doi: 10.1029/2004GL019491.

Snieder, R., 2007, Extracting the Green's function of attenuating heterogeneous acoustic media from uncorrelated waves: Journal of the Acoustical Society of America, **121**, 2637–2643, doi: 10.1121/1.2713673.

Snieder, R., M. Miyazawa, E. Slob, I. Vasconcelos, and K. Wapenaar, 2009, A comparison of strategies for seismic interferometry: Surveys in Geophysics, **30**, 503–523, doi: 10.1007/s10712-009-9069-z.

Snieder, R., K. Wapenaar, and K. Larner, 2006, Spurious multiples in seismic interferometry of primaries: Geophysics, **71**, no. 4, SI111–SI124, doi: 10.1190/1.2211507.

Spetzler, J., and R. Snieder, 2004, The Fresnel volume and transmitted waves: Geophysics, **69**, 653–663, doi: 10.1190/1.1759451.

Thorbecke, J., and G. Drijkoningen, 2007, Efficient computation of passive seismic interferometry: 69th EAGE Conference, London, Expanded Abstracts, P214.

Thorbecke, J., and K. Wapenaar, 2008, Analysis of spurious events in seismic interferometry: 78th Annual International Meeting, SEG, Expanded Abstracts, PSC 1.1.

van der Neut, J., and A. Bakulin, 2009, Estimating and correcting the amplitude radiation pattern of a virtual source: Geophysics, **74**, no. 2, SI27–SI36, doi: 10.1190/1.3073003.

Virieux, J., 1986, P-Sv wave propagation in heterogeneous media — velocity-stress finite-difference method: Geophysics, **51**, 889–901, doi: 10.1190/1.1442147.

Wapenaar, K., 2006, Green's function retrieval by cross-correlation in case of one-sided illumination: Geophysical Research Letters, **33**, L19304–1-6, doi: 10.1029/2006GL027747.

Wapenaar, K., D. Draganov, and J. O. A. Robertsson, eds., 2008, Seismic interferometry: History and present status: SEG Geophysics Reprint Series, **26**.

Wapenaar, K., D. Draganov, J. Thorbecke, and J. Fokkema, 2002, Theory of acoustic daylight imaging revisited: 72nd Annual International Meeting, SEG, Expanded Abstracts, 2269–2272.

Wapenaar, K., and J. Fokkema, 2006, Green's function representations for seismic interferometry: Geophysics, **71**, no. 4, SI33–SI46, doi: 12.1190/1.2213955.

Wapenaar, K., J. Fokkema, and R. Snieder, 2005, Retrieving the green's function in an open system by cross-correlation: A comparison of approaches: The Journal of the Acoustical Society of America, **118**, 5, 2783–2786, doi: 10.1121/1.2046847.

Wapenaar, K., E. Slob, and R. Snieder, 2008, Seismic and electromagnetic controlled-source interferometry in dissipative media: Geophysical Prospecting, **56**, 419–434, doi: 10.1111/j.1365-2478.2007.00686.x.

Wapenaar, K., J. Thorbecke, and D. Draganov, 2004, Relations between reflection and transmission responses of 3-D inhomogeneous media: Geophysical Journal International, **156**, 179–194, doi: 10.1111/gji.2004.156.issue-2.

Wapenaar, K., J. van der Neut, and E. Ruigrok, 2008, Passive seismic interferometry by multidimensional deconvolution: Geophysics, **73**, no. 6, A51–A56, doi: 10.1190/1.2976118.